Near-Infrared-Light-Based Nano-Platform Boosts Endosomal Escape and Controls Gene Knockdown *in Vivo*

Muthu Kumara Gnanasammandhan Jayakumar,[†,∥] Akshaya Bansal,[‡,∥] Kai Huang,[†] Risheng Yao,[⊥] Bing Nan Li,[§,*] and Yong Zhang[†,‡,§,*]

[†]Department of Biomedical Engineering, Faculty of Engineering, National University of Singapore, 117576 Singapore, [‡]NUS Graduate School for Integrative Sciences & Engineering, National University of Singapore, 117456 Singapore, [§]Department of Biomedical Engineering, School of Medical Engineering, Hefei University of Technology, Hefei, Anhui 230009, China, and [⊥]Department of Pharmaceutical Engineering, School of Medical Engineering, Hefei University of Technology, Hefei, Anhui 230009, China. [∥]These authors contributed equally.

ABSTRACT

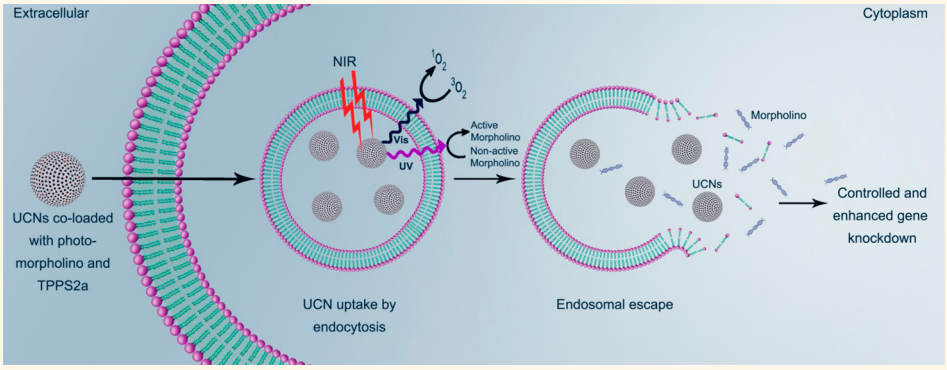

Current nanoparticle-based gene delivery techniques face two major limitations, namely, endosomal degradation and poor cytosolic release of the nanoparticles and nonspecificity of treatment. These limitations can be overcome with certain light-based techniques, such as photochemical internalization to enable endosomal escape of the delivered nanoparticles and light-controlled gene expression to overcome the nonspecific effects. However, these techniques require UV/visible light, which is either phototoxic and/or has low tissue penetration capabilities, thus preventing their use in deep tissues in a clinical setting. In an effort to overcome these barriers, we have successfully demonstrated a light-based gene delivery system that significantly boosts cytosolic gene delivery, with precise control over gene expression and the potential for use in nonsuperficial tissues. Core—shell fluorescent upconversion nanoparticles excited by highly penetrating near-infrared radiation and emitting simultaneously in the ultraviolet and visible ranges were synthesized and used as remote nanotransducers to simultaneously activate endosomal escape and gene knockdown. Gene knockdown using photomorpholinos was enhanced as much as 30% *in vitro* compared to the control without endosomal escape facilitation. A similar trend was seen *in vivo* in a murine melanoma model, demonstrating the enormous clinical potential of this system.

KEYWORDS: upconversion · nanoparticle · photomorpholino · photoactivation · photochemical internalization · mice · gene knockdown

Despite early conceptual promise, gene and genetically mediated therapies have not truly entered medical practice as various issues still prevent desired practical success.[1−3] Various nanoparticles as engineered nonviral vectors have steadily been promising in this regard.[4−6] However, nanoparticles as vectors face two pressing issues: nonspecificity and poor endosomal escape.[7,8]

Several techniques exist for controlled delivery of nucleic acids such as the use of cationic polyplexes,[9] biodegradable polymeric nanoparticles,[10−12] layer-by-layer nanodelivery systems,[13] magnetic nanoparticles for sustained delivery,[14,15] thermoresponsive systems,[16−18] *etc*. However, with these methods, only partial spatial control can be achieved, and there still remains the issue of nontargeted cells being affected. This limits

* Address correspondence to biezy@nus.edu.sg, bingoon@ieee.org.

Received for review February 8, 2014 and accepted April 7, 2014.

Published online April 14, 2014
10.1021/nn500777n

their potential for *in vivo* use since nonspecific gene expression/knockdown can be detrimental. To address the issue of poor cytoplasmic delivery, methods such as use of cationic polymers,[19] cell-penetrating peptides,[20] and pH-sensitive degradable vectors[21] have been explored. Even though the intracellular delivery of nucleic acids is improved using these methods, the issues of specificity still remain.

Photoactivation can provide an elegant solution to the problems mentioned above. It involves the use of molecules inactive by virtue of photosensitive groups incorporated into their structure but are activated when these groups are modified upon irradiation with light of a specific wavelength or *vice versa*. These molecules could be nucleic acids, drugs, *etc*. Photoactivation has been used previously to control gene expression and can be achieved in several ways. One such method involves the use of photocaged nonfunctional nucleic acids such as siRNA or even plasmids, which upon irradiation with UV light release the photolabile group, becoming functional in the process. Another means of achieving photocontrol over gene knockdown is by using a photomorpholino duplex consisting of a sense morpholino with a photolabile moiety and an antisense morpholino that is unmodified. The sense photomorpholino sequesters the antisense morpholino and prevents it from participating in RNA interference (RNAi).[22] Upon irradiation with UV light, the sense photomorpholino is cleaved; this results in the release of the antisense morpholino and thus targeted RNAi-mediated knockdown. Thus, by virtue of site-specific UV irradiation, controlled gene expression/knockdown can be achieved.[23−25] This provides better spatial control as compared to the methods mentioned previously and reduces nonspecific gene expression/knockdown.

An efficient photoactivation technique for improving intracellular delivery of nucleic acids is photochemical internalization (PCI). It involves the use of a small light-sensitive molecule that embeds itself in the endosomes of cells and disrupts the endosomal membrane *via* localized production of reactive oxygen species (ROS) (without causing cell death) upon irradiation with light of a particular wavelength (usually in the visible range). This allows for the nanoparticles to be liberated from the harsh acidic pH conditions in the endosomes/lysosomes, thereby preventing the degradation of the nanoparticles and its cargo and also preventing the nanoparticles from being recycled by the endosomes and deposited out of the cell. Thus, this technique enables precise control of cytoplasmic delivery of the payload without causing any toxicity.[26−30] Even though these photoactivation techniques allow for more specific nucleic acid delivery and better endosomal escape,[31] certain problems limit their use *in vivo*. UV light necessary for uncaging or cleaving nucleic acids such as caged siRNA or photomorpholino is phototoxic and can be potentially carcinogenic. Furthermore, visible light needed for PCI has low tissue penetration. In contrast, near-infrared (NIR) light has excellent tissue penetration capabilities compared to UV or visible light. This is due to the low absorption of NIR light by biological components in tissues. However, NIR light cannot be used to cleave photolabile groups used for light-controlled gene expression and light-sensitive chemicals used for photochemical internalization.

Keeping these issues in mind, we envisioned a simple yet versatile and universal system that could overcome these roadblocks and pave the way for efficient and controlled photoactivation of biomolecules *in vitro* and *in vivo* alike. For this, we synthesized novel NIR-to-UV−vis upconversion nanoparticles (UCNs) made up of a core−shell architecture, which upon NIR excitation emit in the UV and visible range simultaneously, with these emissions potentially capable of exciting multiple photoactive molecules. These core−shell UCNs were used to achieve enhanced gene knockdown through improved endosomal release *via* PCI (using their visible emission). At the same time, the gene knockdown could be controlled using the NIR-to-UV emission of these UCNs. Besides the obvious benefits of using NIR for photoactivation, UCNs have several other desirable properties. Upconversion fluorescence can be generated using inexpensive, commercial continuous wave laser diodes and is exceptionally photostable with low photodamage to cells and proteins.[32] Moreover, UCNs have the ability to be activated in deeper tissues due to the absence of upconversion properties in biological molecules and the higher penetration capability of NIR light in comparison to UV and visible light, thus enabling photoactivation of molecules and long-term, background-free live *in vivo* imaging.[33−36] This makes them an ideal candidate for *in vivo* use. We demonstrate the therapeutic potential of this system by using these UCNs to deliver and remotely activate photomorpholinos, which are difficult to transfect using standard transfection reagents, both *in vitro* and *in vivo* in a murine melanoma model.

RESULTS AND DISCUSSION

The aim of this study was to ascertain whether UCNs could be used to deliver and excite TPPS2a (*meso*-tetraphenylporphine with two sulfonate groups on adjacent phenyl rings, a photosensitizer used in PCI) and a photomorpholino (in this case, anti-STAT3) simultaneously in order to achieve PCI-mediated endosomal escape of the photomorpholino and thus enhance photocontrolled gene knockdown. The graphical abstract gives an overview of the proposed system. The core−shell UCNs were coated with a layer of mesoporous silica and then co-loaded with TPPS2a and photomorpholinos. TPPS2a is a photosensitizer

that absorbs maximally at 413 nm and is used for photochemical internalization. It should not be confused with photosensitizers used for PDT, where the purpose of the photosensitizer is to cause cell death. The loaded photomorpholino is a duplex consisting of a sense photomorpholino and an antisense morpholino hybridized together. Upon irradiation with UV light, the sense photomorpholino gets cleaved, resulting in the release of the antisense morpholino, which can then participate in RNAi. This allows us to achieve spatial and temporal control over gene knockdown using light since, without UV irradiation, the antisense morpholino is effectively sequestered and cannot participate in RNAi. These TPPS2a and photomorpholino duplex-loaded UCNs enter the cell by endocytosis. When these cells are irradiated with NIR at 980 nm, the UCNs emit both UV and visible light simultaneously. The visible light at 413 nm causes TPPS2a to become activated upon which it produces ROS locally. This localized ROS production disrupts the walls of the endosomal vesicles, causing the contents of the endosomes to be released into the cytoplasm. Simultaneously, the UV emission of the UCNs results in the cleavage of the sense photomorpholino, thereby releasing the antisense photomorpholino which can then cause RNAi-mediated knockdown of the target gene, in this case, STAT3.

Core–Shell UCN Synthesis and Characterization. To achieve simultaneous PCI and photocontrolled gene knockdown, UCNs that could emit both UV (to cleave the sense morpholino) and visible light (413 nm to excite TPPS2a) were required. Keeping this in mind, we synthesized core–shell UCNs using a one-pot synthesis method. Figure 1a shows a diagrammatic representation of this core–shell UCN with various coatings. Both the core and the shell are β-$NaYF_4$ crystalline structures with the core doped with ytterbium (Yb^{3+}) and thulium (Tm^{3+}) and the shell doped with Yb^{3+} and erbium (Er^{3+}) to achieve multiple UV and visible emissions, respectively. Figure 1b,c shows transmission electron microscope (TEM) images of the core and core–shell UCNs, respectively. From these images, we can see that the nanoparticle core is below 30 nm in size with a slight increase in size due to the shell. This size is suitable for endosomal uptake.[37] Although the core alone could emit in the UV and blue regions (Figure 1d), emission at 413 nm needed for TPPS2a excitation was absent. The core–shell UCNs, however, had multiple UV and visible emission peaks (Figure 1e), two of which coincided with the photomorpholino and TPPS2a absorption maxima, respectively (Figure 1f). The insets in Figure 1d,e show the visible fluorescence of the NIR-to-UV core and NIR-to-UV–vis core–shell UCNs when irradiated with an NIR laser at 980 nm.

We coated the core–shell nanoparticles with a mesoporous silica layer (Figure 1g) in order to improve their solubility in aqueous solutions and enable loading of molecules onto their surface. We have previously shown that the mesoporous silica coating has a pore size of about about 2 nm.[38] This coating also significantly increases the surface area, which is suitable for loading nucleic acids and photosensitizers, and this was also shown previously by several other groups.[38–40] Henceforth, throughout the article, all references to UCNs stand for mesoporous silica-coated NIR-to-UV/visible core–shell UCNs. We also found that exposure to solutions of different pH values varying from 4.8 (lysosome) to 7.4 (cytosol) did not affect the fluorescence of these nanoparticles (Supporting Information Figure S1) significantly. This was crucial since the UCNs are exposed to conditions of varying pH ranging from physiological pH to acidic pH conditions in endosomes, and if the fluorescence of these UCNs is affected, the ability to photoactivate compounds could be compromised, leading to suboptimal effects.

Cytotoxicity. Having characterized the core–shell UCNs, we conducted cytotoxicity studies before investigating their therapeutic potential. We first evaluated the safety of TPPS2a in B16F0 cells using an MTS assay and found that it was minimally cytotoxic to the cells up to the concentration of 0.8 μg/mL (Figure 2a). We chose 0.7 μg/mL of TPPS2a for future experiments as this concentration produced significant ROS with UCNs as well as being minimally toxic. Another concern while using UCNs is the potential hazard of NIR phototoxicity. Studies on B16F0 cells showed that irradiation with NIR was not harmful to cells since the cell viability was close to 100% at all exposure durations (Figure 2b). In addition, we also tested the cytotoxicity of all combinations of UCNs with TPPS2a/NIR (UCNs, TPPS2a, UCN+TPPS2a, UCN+NIR, TPPS2a+NIR, and UCN+TPPS2a+NIR) and found that in all six cases the cell death was minimal (Figure 2c). The concentration of UCNs used was 500 μg/mL, TPPS2a was 0.7 μg/mL, and irradiation was done using a CW 980 nm NIR laser at a power density of 2.8 W/cm^2 for 8 min. The toxicity arising from the UV emissions of UCNs has already been reported in detail by our group previously, and that was also found to be minimal.[35]

Loading and Release of TPPS2a and Photomorpholino. Following toxicity studies, we conducted experiments to study the loading and release of nucleic acids and TPPS2a from the UCNs. The loading of TPPS2a and photomorpholino for co-loaded UCNs was found to be 1.61 μg TPPS2a/mg UCN and 49.2 μg photomorpholino/mg UCN, respectively (Table 1). These values were calculated by measuring the initial amount of TPPS2a and the photomorpholino in the solution used for loading and subtracting from it the amount of the two in the supernatant postloading. The UCNs were vacuum-dried after loading and stored at 4 °C and resuspended only prior to use. The cumulative release of both the molecules in deionized (DI) water was sustained over several hours and is shown in Figure 3a.

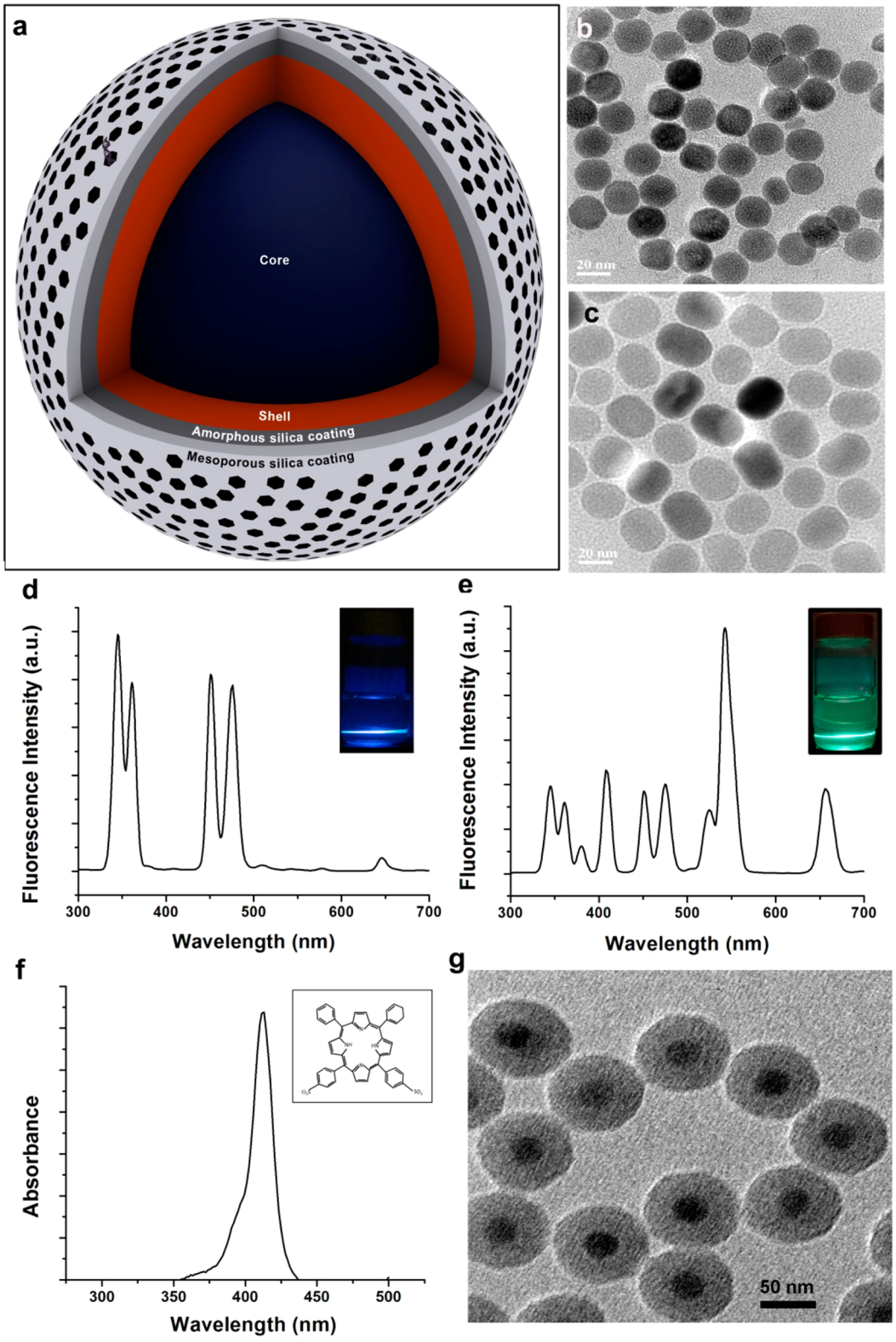

Figure 1. (a) Schematic showing the structure of core–shell UCNs and its various coatings. (b) Transmission electron micrographs of NIR-to-UV core and (c) NIR-to-UV/vis core–shell UCNs. (d) Fluorescence emission spectrum of NIR-to-UV UCN core, where inset shows the total fluorescence of the nanoparticles in a cuvette when irradiated with NIR at 980 nm, and (e) fluorescence emission spectrum of NIR-to-UV/vis core–shell UCNs, where inset shows the total fluorescence of the nanoparticles in a cuvette when irradiated with NIR at 980 nm. (f) Absorbance spectrum of TPPS2a with its structure in the inset and (g) mesoporous silica-coated NIR-to-UV/vis core–shell UCNs.

UCN-Mediated Photomorpholino Cleavage and TPPS2a Activation. We conducted experiments to determine whether the UV emission from UCNs was sufficient to cleave the sense photomorpholino. Photomorpholinos

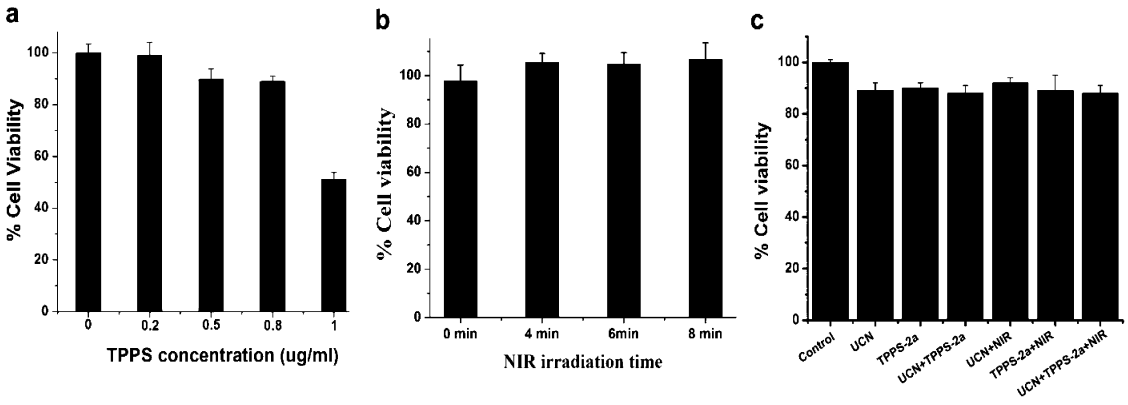

Figure 2. (a) Effect of varying concentrations of TPPS2a on the viability of B16F0 cells. (b) Phototoxicity of B16FO cells exposed to different durations of 980 nm NIR laser. (c) Cytotoxicity of B16F0 cells exposed to different combinations of UCNs, TPPS2a, and NIR (UCNs alone, TPPS2a alone, UCN+TPPS2a, UCN+NIR, TPPS2a+NIR and UCN+TPPS2a+NIR).

TABLE 1. Characteristics of Mesoporous Silica-Coated NIR-to-UV/Vis Core–Shell UCNs

hydrodynamic diameter (nm)	polydispersity index	ζ-potential (mV)	loading efficiency (per mg of UCN)	
122	0.216	−20.3	1.61 μg of TPPS2a	49.2 μg of photomorpholino

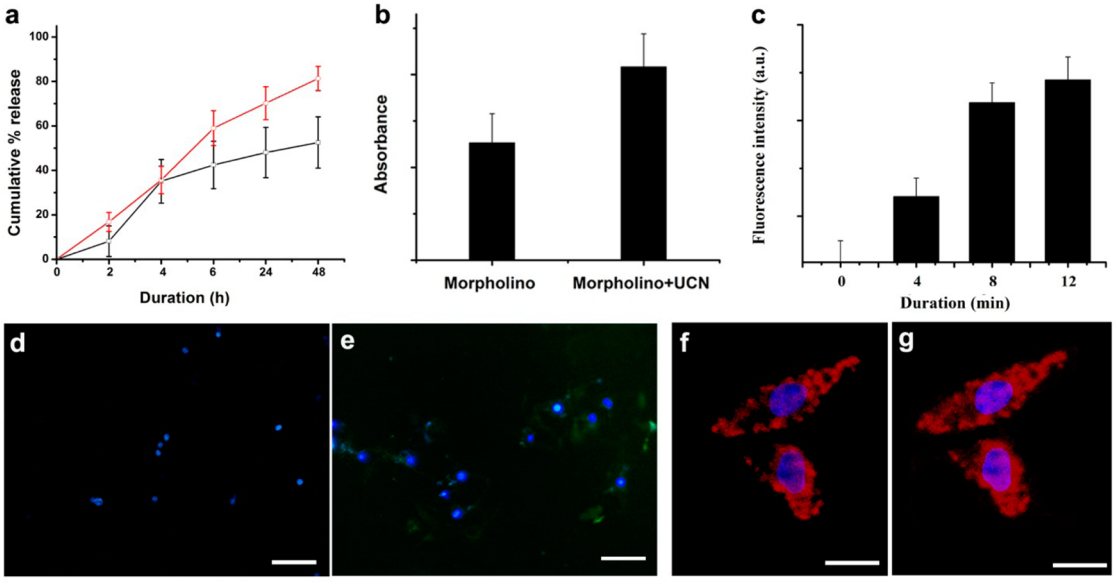

Figure 3. (a) Cumulative percentage release of photomorpholino (red) and TPPS2a (black) from core–shell UCNs over time. (b) Absorbance readings at 260 nm of photomorpholinos incubated with and without UCNs post-NIR irradiation; increase in absorbance indicates the increase in morpholino fragments due to (UCN-emitted) UV photolysis. (c) ROS production by UCNs (TPPS2a-loaded) after irradiation with NIR and determined by APF. (d) Fluorescence images after incubation with Image-iT LIVE Green ROS detection reagent of untreated cells and (e) cells treated with UCNs+TPPS2a post-NIR irradiation of 8 min at a power density of 2.8 W/cm^2. Cells were counterstained with DAPI (scale bar: 50 μm). Green fluorescence indicates the production of ROS. Distribution of UCNs before (f) and after (g) NIR irradiation (scale bar: 5 μm): UCNs, red; DAPI, blue. More diffuse pattern shows cytosolic release after endosomal escape.

were taken in two separate cuvettes, with one containing UCNs and one without. Both samples were irradiated with NIR at 980 nm. The sample that contained UCNs showed a higher absorption at 260 nm post-irradiation. This was possibly due to the presence of more nucleic acid fragments in solution due to the photolysis of the sense photomorpholino upon exposure to the upconverted UV light produced by the UCNs when irradiated with NIR (Figure 3b), indicating successful photolysis *via* UCN UV emission.

The visible emission peak of UCNs coincides with the excitation peak of TPPS2a (413 nm). To determine whether these core–shell UCNs could indeed activate TPPS2a, we measured the ROS produced after NIR irradiation for UCNs loaded with TPPS2a in distilled water (Figure 3c) and in cells (Figure 3d,e). Increase in

ROS production was observed with increase in the duration of NIR irradiation in distilled water; however, in cells, the ROS production was localized and minimal (as can be seen from the faint green fluorescence of the ROS indicator). This is desirable as the goal of using this photosensitizer is not to cause cell death but to enhance endosomal escape *via* localized production of ROS in the endosomes.[41] Also, TPPS2a did not affect the stability of the photomorpholino (Supporting Information Figure S2) since the absorbance of the nucleic acid remained unchanged even after 24 h of co-incubation with TPPS2a. In addition, the ROS produced by TPPS2a did not affect the functional integrity of the nucleic acid (Supporting Information Figure S3).

Endosomal Escape. Next, we wanted to ascertain whether UCNs localized in the endosome and whether the use of TPPS2a resulted in an enhanced endosomal release. Figure 3f,g shows the distribution of core−shell UCNs loaded with TPPS2a in the same field of cells at time 0 and 10 min after irradiation with NIR, respectively. Initially, the UCNs are present in clumps and not very well dispersed inside the cells. However, only 10 min after irradiation, we could see a marked change in the distribution of UCNs, indicating improved endosomal release.

***In Vitro* STAT3 Knockdown.** To test this system *in vitro*, we used B16F0 cells in which STAT3 is aberrantly activated. Consistent activation of STAT3 plays a major role in cancer progression, and knockdown of STAT3 has been found to enhance cell death, improve immune response, and bring about tumor regression.[42,43] We used UCNs co-loaded with TPPS2a and anti-STAT3 photomorpholino (double-stranded: sense photomorpholino and unmodified antisense strand) to target STAT3 in a specific manner. Initially, the effect of TPPS2a on the cytosolic release of nanoparticles and the mechanism of action was studied by incubating B16F0 cells with TPPS2a-loaded UCNs and UCNs alone for 8 h at 37 and 4 °C, respectively. After 8 h of incubation, the cells were washed thoroughly and trypsinized. Using fluorescence spectrometry, the UCN concentration was then estimated in the cell suspension. The fluorescence intensity was similar for cells with UCNs alone and those incubated with TPPS2a and UCNs, indicating similar uptake (Supporting Information Figure S4). These samples were then irradiated with NIR for 8 min and replated, and after overnight incubation, the concentration of nanoparticles inside the cells and in the media (supernatant) were quantified using fluorescence spectrophotometry. The samples incubated at 4 °C (endocytosis is arrested) had very minimal uptake with or without TPPS2a, indicating that endocytosis is required for cellular uptake of UCNs. For the samples incubated at 37 °C, there was an increase in cellular concentration of the UCNs loaded with TPPS2a when compared to those without TPPS2a, as shown in Figure 4a. Also, the extracellular concentration of UCNs (in the supernatant) in cells

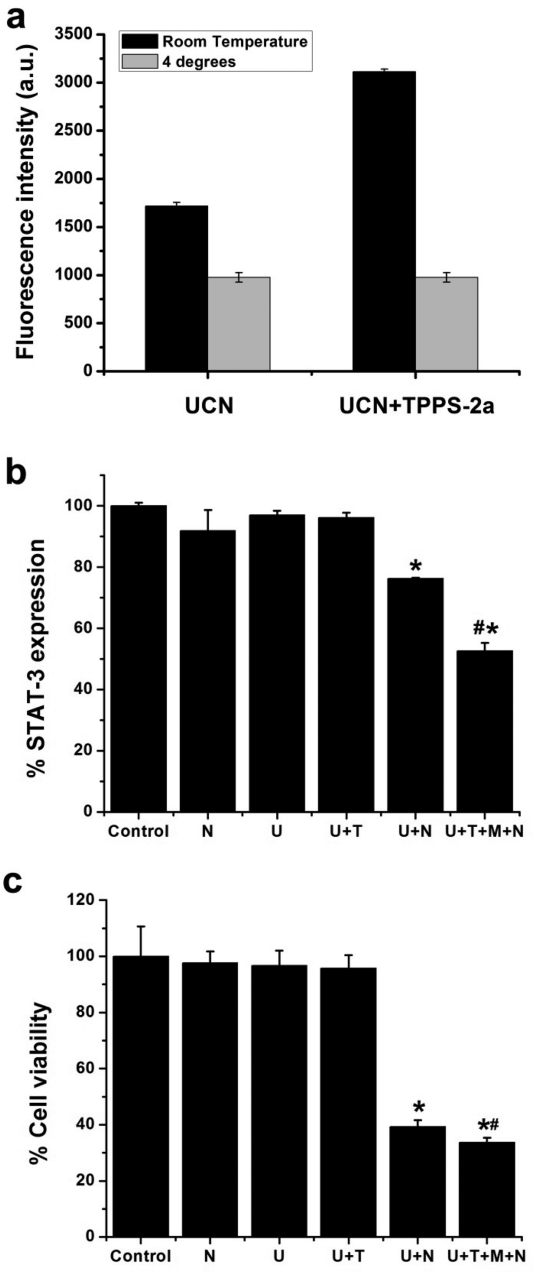

Figure 4. (a) Fluorescence intensity of UCNs in B16F0 cell suspension with and without TPPS2a at normal temperature and 4 °C, 24 h after irradiation with NIR at 980 nm. (b) Percentage STAT3 expression and (c) cell viability of B16F0 cells exposed to different combinations of UCNs, TPPS2a, morpholinos, and NIR. *$p < 0.05$ between control and test groups. #$p < 0.05$ between UCN+morpholino and UCN+morpholino+TPPS2a.

treated with UCNs alone was higher than those with UCNs loaded with TPPS2a (Supporting Information Figure S5). Since the initial UCN uptake amount was similar for both groups, the results when taken together suggested greater UCN retention in the cells with the use of TPPS2a. A larger amount of UCNs in the supernatant of the control group (UCNs only) suggested that the cells could indeed exocytose the nanoparticles if endosomal escape does not occur.[44]

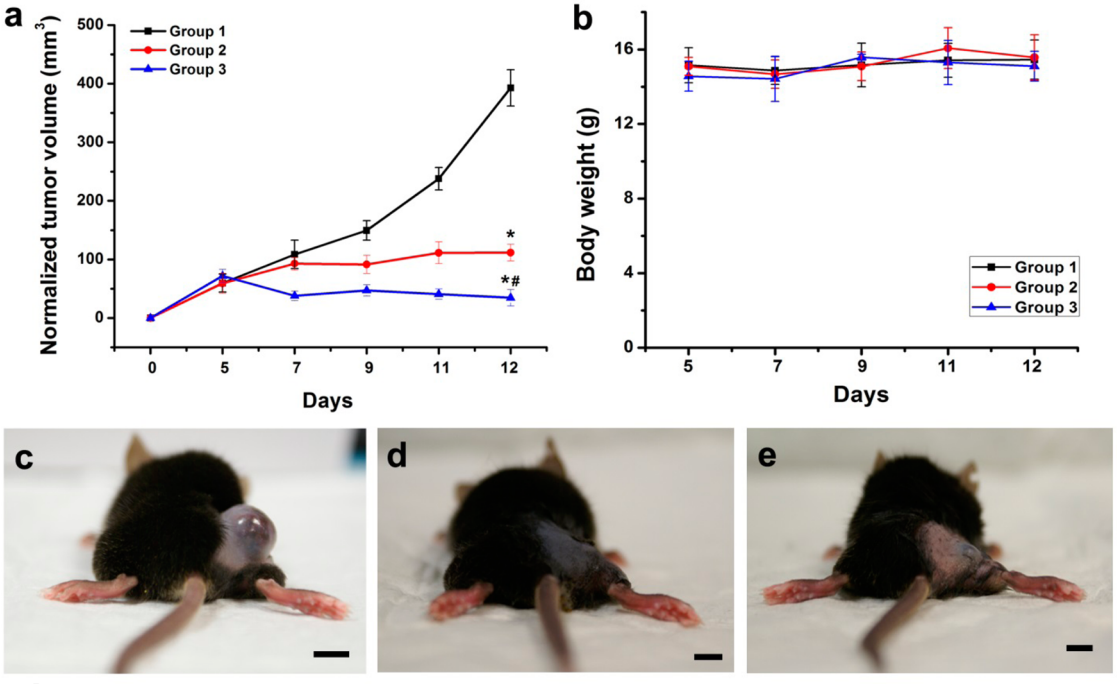

Figure 5. Effect of STAT3 knockdown in a murine model of melanoma. Change in tumor volume (a) and body weight (b) as a function of time to assess the effectiveness of treatment. Values are means ± SEM (n = 6 mice per group). Group 1, saline control; group 2, UCNs loaded with photomorpholinos and irradiated with NIR laser; group 3, UCNs co-loaded with photomorpholinos and TPPS2a and irradiated with NIR laser. Representative gross photos of a mouse from each group 1−3 (c−e). Scale bar: 1 cm; *p < 0.05 between group 1 and groups 2,3; #p < 0.05 between group 2 and group 3.

These results indicate that UCNs enter the cells through endocytosis and escape the endosome *via* PCI, thereby effectively increasing the intracellular concentration of UCNs.

Next, experiments were conducted to determine if UCNs could be used for photocontrolled gene knockdown and whether enhancement in cellular uptake of UCNs *via* PCI increased the effectiveness of gene knockdown. For this, B16F0 cells were treated with UCNs loaded with STAT3 photomorpholino, with or without TPPS2a, and irradiated with NIR. Figure 4b shows that UCNs were able to activate photomorpholinos in both cases; however, the STAT3 knockdown is significantly higher in the sample with TPPS2a (p = 0.0063). The corresponding cytotoxicity of the samples after STAT3 knockdown is given in Figure 4c, and their bright-field images are given in Supporting Information Figure S6. It can be seen that there is a significant increase in cell death with PCI as compared to without, which is in line with the STAT3 knockdown results (p = 0.0285). However, it was seen that, for both STAT3 knockdown and STAT3-induced cytotoxicity, control groups, namely, cells treated with NIR irradiation alone, UCNs, and UCNs loaded with TPPS2a, did not cause significant changes.

***In Vivo* STAT3 Knockdown.** To demonstrate the efficacy of this system *in vivo*, we chose mouse as a model organism. We used the STAT3 photomorpholinos mentioned previously to knockdown STAT3 in a tumor model of melanoma. Tumors were induced in mice by injecting B16F0 cells subcutaneously. UCNs loaded with STAT3 photomorpholinos with or without TPPS2a were administered on day 5 and day 8, and the tumors were irradiated with a NIR laser. Control mice received saline injections. From Figure 5a, we can see that there is a significant reduction in tumor volume in mice that had been treated with UCNs loaded with photomorpholino (group 2) and with co-loaded (with photomorpholino and TPPS2a) UCNs (group 3) as compared to mice that had been given saline (group 1) with a p value of 0.14351 and 0.04134, respectively. Also, there was a marked decline in tumor volume in mice treated with UCNs co-loaded with photomorpholino and TPPS2a (group 3) as compared to those treated with photomorpholino-loaded UCNs alone (p value 0.00383). This indicated that core−shell UCNs could be used for simultaneous PCI and photocontrollable gene expression and that this significantly enhanced the therapeutic effect. The mice in all these groups were otherwise healthy as shown by their body weight[45,46] in Figure 5b. Representative photographs of mice in different groups are given in Figure 5c−e.

Several other controls were also included (treatment with UCNs alone, NIR alone, UCNs loaded with photomorpholino but without NIR irradiation, UCNs co-loaded with photomorpholino and TPPS2a but without NIR irradiation), as shown in Supporting Information Figure S7. There was no significant reduction in tumor size in any of these control groups as compared to the saline-treated mice. Analysis of the tissue samples harvested from these mice indicated lower STAT3 levels in mice treated with photomorpholino-loaded UCNs

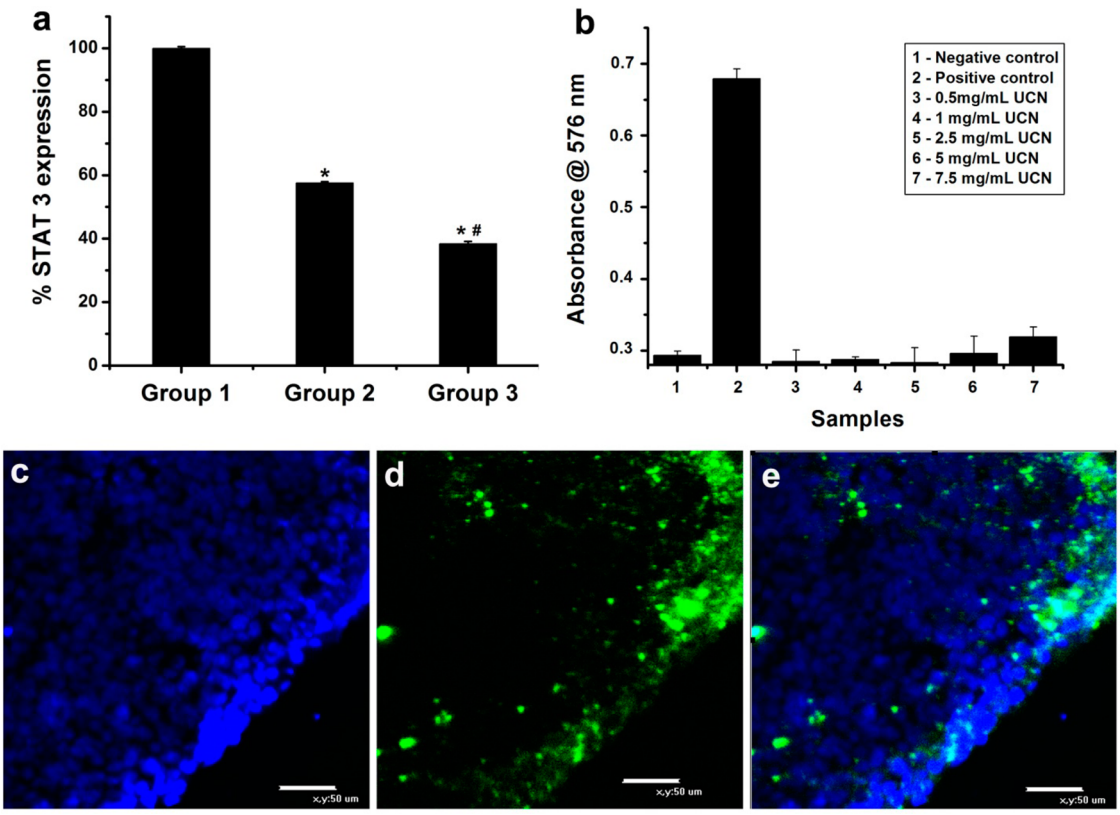

Figure 6. (a) Expression of STAT3 in tumor tissues from groups 1−3 analyzed by ELISA after harvesting. (b) Hemolytic activity of different concentrations of UCNs in mice blood. (c) Imaging of UCNs in tumor tissue sections, DAPI, (d) UCN fluorescence, (c) merge of c and d. Scale bar = 50 μm; *p < 0.05 between group 1 and groups 2,3; #p < 0.05 between group 2 and group 3.

(group 2) and co-loaded (photomorpholino and TPPS2a) UCNs (group 3) as compared to the control ($p = 1.87187 \times 10^{-7}$ and 1.87187×10^{-7}, respectively) as shown in Figure 6a. Also, STAT3 levels were significantly lower in case of co-loaded (photomorpholino and TPPS2a) UCNs than photomorpholino-loaded UCNs ($p = 1.28959 \times 10^{-5}$), which reaffirmed the previous results. Also, UCNs did not result in significant hemolysis (Figure 6b), reaffirming the relative safety of their use. From Figures 6c−e, it can be seen that UCNs can be detected in the tumor tissue, thus potentially enabling background-free *in vivo* imaging.

CONCLUSION

Nanoparticle-based gene therapy faces debilitating hurdles like poor endosomal escape and limited control over gene expression. Even though photocontrol of gene expression and endosomal release have been described previously in literature, which overcome these issues, the clinical application of these solutions is limited due to the toxic and low penetrating light sources used. In this study, a unique solution has been provided to address this limitation by developing a nano-platform, which can utilize highly penetrating NIR light for photoactivation. This is believed to be the first report of using such a system for simultaneous gene delivery, photocontrolled gene expression, and photochemical internalization *in vitro* and *in vivo* with negligible toxicity and additional background-free imaging capabilities.

Our results demonstrate that this UCN-based system significantly enhances the delivery of photomorpholinos *via* PCI *in vitro* as well as in complex *in vivo* environments, thereby improving the therapeutic efficacy of such nucleic-acid-based treatment modalities. Thus, we have addressed major bottlenecks of *in vivo* gene delivery, primarily that of endosomal escape and non-specificity and demonstrated the tremendous potential of this system in furthering such RNAi-based treatment modalities from the bench to bedside. In addition, the versatility of this nano-platform potentially allows it to be used in other disease models where gene therapy could be applicable.

EXPERIMENTAL SECTION

Materials. B16F0 cells were purchased from the American Type Culture Collection (ATCC). All chemicals for nanoparticle synthesis and surface coating like yttrium chloride, thulium chloride, ytterbium chloride, *N*-[3-(trimethoxysilyl)propyl]-ethylenediamine (AEAPTMS), acetic acid, and cyclohexane were purchased from Sigma-Aldrich (Singapore). Photomorpholinos were purchased from Gene Tools, LLC, USA. TPPS2a was

purchased from PCI Biotech (Oslo, Norway). CellTiter 96 AQ_{ueous} One Solution cell proliferation assay for cytotoxicity testing was purchased from Promega (Madison, WI, USA). Image-iT LIVE ROS kit was purchased from Molecular Probes, USA. Thermo Scientific Pierce STAT3 in-cell ELISA kit was used for *in vitro* STAT3 analysis and STAT3 InstantOne ELISA kit (eBioscience, Inc., Belgium) for *in vivo* STAT3 analysis.

Synthesis of Mesoporous-Coated Core−Shell UCNs. Synthesis of core−shell UCNs was done by slight modification of an earlier method. In brief, a β-$NaY_{74.7}F4{:}Yb_{25}{,}Tm_{0.3}$ core was synthesized using a thermal decomposition method as described by our group previously and then purified and dispersed in cyclohexane. Briefly, 0.78 M of YCl_3, 0.20 M of $YbCl_3$, and 0.2 M of $ErCl_3$ were taken in a 50 mL three-necked flask and heated until dryness. Then, 6 mL of oleic acid and 15 mL of 10-octadecene were added, and the solution was heated until 150 °C. After 30 min, the solution was cooled to 50 °C and the previously synthesized $NaYF_4$:Yb,Tm core was added and the resulting mixture was heated to 110 °C for 30 min to remove cyclohexane. Once the cyclohexane was removed, the solution was cooled to 50 °C and 0.1 g of NaOH and 0.1482 g of NH_4F in 5 mL of methanol were added. Subsequently, the solution was heated to 110 °C for 15 min and then degassed at the same temperature for next 20 min. The solution was then heated at 300 °C under argon atmosphere for 1 h, cooled to room temperature, purified, and redispersed in cyclohexane.

Mesoporous coating of the synthesized core−shell UCNs was done by calcination method. Briefly, the UCNs were coated with a silica layer as follows: 1 mL of Igepal CO-520 and 18.4 mL of cyclohexane were added to 1.6 mL of 0.05 M UCNs and homogenized under ultrasonication. To the solution, were added 160 μL of 30% NH_4OH and 40 μL of TEOS (tetraethyl orthosilicate) and shaken for 2 days. After 2 days, the resulting silica-coated UCNs were purified using acetone and ethanol. Subsequently, a second coating of mesoporous silica was done. To the as-synthesized silica-coated UCNs were added 2.6 mL of 30% NH_4OH, 13 mL of ethanol, 260 μL of TEOS, and 104 μL of C18 TMS (octadecyltrimethoxysilane 90%) and shaken for 6 h. The resulting homogeneous white solution was dried in hot-air oven at 60 °C overnight and then subsequently calcinated at 500 °C in a furnace for 6 h. The dried powder was then milled and subsequently dissolved in deionized water. Due to the multiple coating steps and possible UCN losses in these steps, it is often difficult to express the molarity of the UCNs obtained; instead, the concentration in μg/mL (weight/volume) is often used.[47,48]

Characterization of UCNs. TEM images were recorded on a JEOL 2010F transmission electron microscope (JEOL Ltd., Tokyo, Japan) operating at an acceleration voltage of 200 kV. Fluorescence spectra of UCNs were recorded on a Hitachi F-500 fluorescence spectrophotometer (Hitachi High-Technologies Corporation, Tokyo, Japan) equipped with an NIR continuous wave laser with emission at 980 nm (Photonitech (Asia) Pte. Ltd., Singapore).

Cell Culture. B16F0 cells were grown in DMEM culture medium supplemented with 10% FBS, 100 units/mL of penicillin, and 100 μg/mL of streptomycin and maintained in a humidified, 5% carbon dioxide (CO_2) atmosphere at 37 °C.

Cell Viability Assay. B16F0 cells were treated with different conditions and then incubated for 24 h before being assayed for cell viability using an MTS assay as per manufacturer's instructions.

Co-loading onto and Release of TPPS2a and Photomorpholino from UCNs. To 1 mL of 1 mg/mL UCNs was added 25 nmol each of sense photomorpholino and antisense morpholino against STAT3 (Gene Tools, LLC), and the mixture shaken at 1000 rpm for 2 h protected from light. Then, 24 μL of TPPS2a (PCI Biotech, Norway) was added and shaken for another hour. The solution was then centrifuged at 8000 rpm for 10 min to separate the loaded UCNs. The supernatant was removed and the absorbance of photomorpholinos and TPPS2a measured. Comparing the amount of the two in the supernatant to the initial concentration added, we were able to calculate the amount of TPPS2a and photomorpholino loaded/mg of these core−shell UCNs. After loading, the UCNs were vacuum-dried and stored at 4 °C and resuspended immediately prior to use.

For release studies, the UCNs co-loaded with TPPS2a and photomorpholino were resuspended in DI water. After 2 h, these UCNs were spun down, the supernatant collected, and the amount of photomorpholino and TPPS2a measured in the supernatant. This was done at 2, 4, 6, 24, and 48 h. Using the data obtained and comparing it to the amount of the two molecules loaded initially, we plotted a cumulative release graph to indicate the release profile of the two molecules. This experiment was repeated twice for independent validation.

Photolysis of Photomorpholino through UCN UV Emission. To ascertain whether the UV emission from mesoporous silica-coated core−shell UCNs was sufficient to cause photolysis of the sense photomorpholino, two samples of these photomorpholinos were prepared, with one containing 0.5 mg/mL UCNs and one without. The concentration of photomorpholinos in the two samples was the same. These samples were then irradiated with NIR for 8 min, and then the absorbance was measured at 260 nm (absorption maximum for nucleic acids). Photolysis would typically cause an increase in the number of nucleic acid fragments and subsequently an increase in the absorbance at 260 nm.

ROS Detection in Solution. Two milliliters of 1 mg/mL TPPS2a-loaded UCN solution was taken in a cuvette. For control, two other cuvettes contained water and unloaded UCN solution. To each of the three cuvettes was added 2 μL of APF. Then, 100 μL of sample was taken from each of the cuvettes and spun down at 12 000 rpm for 5 min. Fifty microliters of supernatant was taken from each and put in a dark (opaque) 96-well plate (protected from light). The fluorescence of the samples was recorded (490/515 ex/em). The three cuvettes were then irradiated at different time points, and after each time point, 100 μL of sample was taken from each of the cuvettes and processed as mentioned above. The fluorescence readings were then plotted against time to indicate amount of ROS produced by TPPS2a with increasing duration of NIR exposure.

Using Image-iT Green Live ROS Detection Kit. B16F0 cells were incubated with 0.5 mg/mL of UCNs loaded with TPPS2a overnight. The excess nanoparticles were then washed off the cells, and the cells were irradiated using a 980 nm NIR laser. The ROS generated in the cells was detected using an Image-iT LIVE ROS kit as per manufacturer's instruction. The cells were also counterstained with DAPI and imaged using a confocal laser scanning microscope (Nikon C1 Confocal, Nikon, Tokyo, Japan) specially fitted with a CW 980 nm laser excitation source (Opto-Link Corp., Hong Kong). All images were taken using the same gain and pixel dwell (30 μs).

Cellular Uptake of UCNs. B16F0 cells were incubated with mesoporous silica-coated core−shell UCNs either loaded with TPPS2a or without. One set of the above-mentioned sample was incubated at 4 °C and another at 37 °C. After 8 h of incubation, all the samples were irradiated with a 980 nm CW NIR laser for 8 min. The samples were then incubated overnight at the respective temperatures. The cells were washed three times to remove the UCNs present in the supernatant and the surface of the cells. The cells were then trypsinized, and the fluorescence emission of the UCNs was recorded using a Hitachi F-500 fluorescence spectrophotometer (Hitachi High-Technologies Corporation, Tokyo, Japan) equipped with an NIR continuous wave laser with emission at 980 nm (Photonitech (Asia) Pte. Ltd., Singapore).

Redistribution of UCNs Following PCI. B16F0 cells were plated on a 24-well plate. After overnight incubation, TPPS2a-loaded UCNs were added to the test and control wells. After 8 h of incubation, the medium was removed and the cells were incubated with 0.1 mg/mL concanavalin A-Alexa Fluor 488 in culture medium and 0.01 mg/mL DAPI for 30 min at 37 °C. They were then washed three times with PBS and replenished with fresh culture medium. The cells were then imaged using a confocal microscope (Nikon C1 Confocal, Nikon, Tokyo, Japan) (UCNs, the cell stained with concanavalin A and nuclei stained with DAPI). Concanavalin emission was pseudocolored to red to distinguish from the green emission of UCNs. Merging of the two images showed localization of UCNs in the cells. Another set of wells was irradiated with a CW 980 nm NIR laser for 8 min and was imaged similarly after 10 min.

ELISA for STAT3 Knockdown. B16F0 cells (in which STAT3 is aberrantly activated) were incubated with UCNs loaded with

double-stranded (sense and antisense) anti-STAT3 photomorpholino in two columns (3 wells/column) of a 96-well plate and UCNs co-loaded with photomorpholino and TPPS2a in two other columns. The concentration of UCNs/well was 500 μg/mL. For control, cells were plated without the nanoparticles. After 6−8 h of incubation, the cells in two columns (one with UCNs loaded with photomorpholino alone and one with co-loaded UCNs) were irradiated for 8 min with 980 nm (NIR) radiation, respectively. After this, the plate was incubated for another 72 h and then ELISA was performed according to the manufacturer's instructions.

***In Vivo* Studies.** This study conforms to the Guide for the Care and Use of Laboratory Animals published by the National Institutes of Health, USA, and protocol approved by the Institutional Animal Care and Use Committee (IACUC), National University of Singapore. All experiments used C57BL/6 mice of 4−6 weeks old, and anesthesia was done by intraperitoneal injection of ketamine (75 mg/kg body weight) and medetomidine (1 mg/kg body weight).

***In Vivo* Gene Therapy Using UCNs.** Tumors were first developed in C57BL/6 mice by subcutaneously implanting 3×10^6 B16F0 cells suspended in 100 μL of serum-free DMEM in the lower flanks of the mice. Six days after inoculation of tumor cells, the mice were randomly divided into different groups. Each group was then injected with 100 μL of the following intratumorally. Group 1, saline; group 2, UCNs loaded with anti-STAT3 photomorpholinos; group 3, UCNs co-loaded with TPPS2a and anti-STAT3 photomorpholinos. Laser treatment was performed on groups 2 and 3, 6 h after injection by irradiating the tumor region with a CW 980 nm laser (EINST Technology Pte Ltd., Singapore) at a laser power density of 300 mW/cm^2 and exposure time of 40 min. A second dose of the above PDT treatment was repeated 3 days following the first. Tumor size and body weight was measured three times a week. The tumor volume, V, was calculated using the formula $V = (L \times W^2)/2$, as reported previously,[49,50] where L is the longest dimension of the tumor and W is the perpendicular width to L.

Evaluating the Expression of STAT3 in Tumors. At the end of study, three mice were chosen randomly from each group and euthanized. The tumors (50 mg each) were then homogenized, and the homogenate was centrifuged at 12 000 rpm for 20 min. The supernatant was taken and used for further analysis. Expression of STAT3 was measured using ELISA.

UCN Imaging in Tumors. The tumors were harvested and snap frozen using liquid nitrogen. They were cryosectioned at 10 μm thickness onto slides and fixed using paraformaldehyde. The sections were then counterstained with DAPI, and the fluorescence of DAPI and UCNS was imaged using a fluorescence confocal microscope (Nikon C1 Confocal, Nikon, Tokyo, Japan).

Hemolytic Activity Test. rRBCs were washed with PBS three times and subjected to 25× volumetric dilutions in PBS to achieve 4% blood content (by volume). Different concentrations of mesoporous silica-coated UCNs were diluted in saline. Equal volume of blood and the UCN solution was mixed together, and the mixture was incubated at 37 °C for 1 h to allow for the interactions between rRBC and UCNs. After incubation, the mixture was centrifuged at 4000 rpm for 5 min, and the supernatant was transferred into a 96-well microplate. The hemoglobin release was measured spectrophotometrically by measuring the absorbance of the samples at 576 nm using a microplate reader. Two control groups were provided for this assay: untreated rRBC suspension (as negative control) and rRBC suspension treated with 0.1% Triton-X (as positive control). Each assay was performed in triplicate.

Statistical Analysis. The normality of the populations was initially tested. The mean values of the different treatment groups were then statistically compared to that of the control group using ANOVA for normally distributed populations and Kruskal−Wallis ANOVA for populations that were not normally distributed using OriginPro 8.1; $p < 0.05$ was considered statistically significant.

Conflict of Interest: The authors declare no competing financial interest.

Acknowledgment. We thank Niagara Muhammad Idris for technical support and useful discussions and Selva Rajan for support in preparing the schematic illustrations. Financial support from Singapore A*STAR Biomedical Research Council (Grant No. R-397-000-119-305) and National University of Singapore is also gratefully acknowledged. We also acknowledge the funding support from the National Natural Science Foundation of China (Grant No. 31328009) and the Fundamental Research Funds for the Central Universities (Grant No. 2013HGCH0001).

Supporting Information Available: Stability of UCNs and siRNA and TPPS2a co-loaded UCNs, functional integrity of morpholinos post-ROS exposure, UCN fluorescence in cells after overnight incubation of UCNs with cells and before NIR irradiation, UCN fluorescence in the supernatant measured 24 h postirradiation, bright-field images of B16F0 cells transfected with UCNs loaded with morpholinos and TPPS2a, tumor at day 12 in mice treated with morpholino-loaded UCNs (with out NIR), NIR alone, UCNs loaded with morpholino and TPPS2a but without NIR irradiation, and NIR irradiation alone (control *in vivo* experiments). This material is available free of charge *via* the Internet at http://pubs.acs.org.

REFERENCES AND NOTES

1. Verma, I. M.; Somia, N. Gene Therapy: Promises, Problems and Prospects. *Nature* **1997**, *389*, 239–242.
2. Pecot, C. V.; Calin, G. A.; Coleman, R. L.; Lopez-Berestein, G.; Sood, A. K. RNA Interference in the Clinic: Challenges and Future Directions. *Nat. Rev. Cancer* **2011**, *11*, 59–67.
3. Kay, M. A. State-of-the-Art Gene-Based Therapies: the Road Ahead. *Nat. Rev. Genet.* **2011**, *12*, 316–328.
4. Shan, Y.; Luo, T.; Peng, C.; Sheng, R.; Cao, A.; Cao, X.; Shen, M.; Guo, R.; Tomás, H.; Shi, X. Gene Delivery using Dendrimer-Entrapped Gold Nanoparticles as Nonviral Vectors. *Biomaterials* **2012**, *33*, 3025–3035.
5. Zheng, D.; Giljohann, D. A.; Chen, D. L.; Massich, M. D.; Wang, X.-Q.; Iordanov, H.; Mirkin, C. A.; Paller, A. S. Topical Delivery of siRNA-based Spherical Nucleic Acid Nanoparticle Conjugates for Gene Regulation. *Proc. Natl. Acad. Sci. U.S.A.* **2012**, *109*, 11975–11980.
6. Bhakta, G.; Sharma, R. K.; Gupta, N.; Cool, S.; Nurcombe, V.; Maitra, A. Multifunctional Silica Nanoparticles with Potentials of Imaging and Gene Delivery. *Nanomedicine* **2011**, *7*, 472–479.
7. Montier, T.; Delepine, P.; Pichon, C.; Ferec, C.; Porteous, D.; Midoux, P. Non-Viral Vectors in Cystic Fibrosis Gene Therapy: Progress and Challenges. *Trends Biotechnol.* **2004**, *22*, 586–592.
8. Li, S.; Huang, L. Nonviral Gene Therapy: Promises and Challenges. *Gene Ther.* **2000**, *7*, 31–34.
9. Davis, M. E. The First Targeted Delivery of siRNA in Humans *via* a Self-Assembling, Cyclodextrin Polymer-based Nanoparticle: from Concept to Clinic. *Mol. Pharmaceutics* **2009**, *6*, 659–668.
10. Vandenbroucke, R. E.; De Geest, B. G.; Bonné, S.; Vinken, M.; Van Haecke, T.; Heimberg, H.; Wagner, E.; Rogiers, V.; De Smedt, S. C.; Demeester, J.; *et al.* Prolonged Gene Silencing in Hepatoma Cells and Primary Hepatocytes after Small Interfering RNA Delivery with Biodegradable Poly(β-amino esters). *J. Gene Med.* **2008**, *10*, 783–794.
11. Lee, J.-S.; Green, J. J.; Love, K. T.; Sunshine, J.; Langer, R.; Anderson, D. G. Gold, Poly(α-amino ester) Nanoparticles for Small Interfering RNA Delivery. *Nano Lett.* **2009**, *9*, 2402–2406.
12. Morachis, J. M.; Mahmoud, E. A.; Sankaranarayanan, J.; Almutairi, A. Triggered Rapid Degradation of Nanoparticles for Gene Delivery. *J. Drug Delivery* **2012**, 291219.
13. Lee, S. K.; Han, M. S.; Asokan, S.; Tung, C.-H. Effective Gene Silencing by Multilayered siRNA-Coated Gold Nanoparticles. *Small* **2011**, *7*, 364–370.
14. Del Pino, P.; Munoz-Javier, A.; Vlaskou, D.; Rivera Gil, P.; Plank, C.; Parak, W. J. Gene Silencing Mediated by Magnetic Lipospheres Tagged with Small Interfering RNA. *Nano Lett.* **2010**, *10*, 3914–3921.
15. Chorny, M.; Fishbein, I.; Tengood, J. E.; Adamo, R. F.; Alferiev, I. S.; Levy, R. J. Site-Specific Gene Delivery to

Stented Arteries using Magnetically Guided Zinc Oleate-based Nanoparticles Loaded with Adenoviral Vectors. *FASEB J.* **2013**, *27*, 2198–2206.
16. Chen, K.-J.; Liang, H.-F.; Chen, H.-L.; Wang, Y.; Cheng, P.-Y.; Liu, H.-L.; Xia, Y.; Sung, H.-W. A Thermoresponsive Bubble-Generating Liposomal System for Triggering Localized Extracellular Drug Delivery. *ACS Nano* **2012**, *7*, 438–446.
17. Dias, J. T.; Moros, M.; del Pino, P.; Rivera, S.; Grazú, V.; de la Fuente, J. M. DNA as a Molecular Local Thermal Probe for the Analysis of Magnetic Hyperthermia. *Angew. Chem.* **2013**, *125*, 11740–11743.
18. Munoz Javier, A.; Del Pino, P.; Bedard, M.; Ho, D.; Skirtach, A.; Sukhorukov, G.; Plank, C.; Parak, W. Photoactivated Release of Cargo from the Cavity of Polyelectrolyte Capsules to the Cytosol of Cells. *Langmuir* **2008**, *24*, 12517–12520.
19. Shrestha, R.; Elsabahy, M.; Florez-Malaver, S.; Samarajeewa, S.; Wooley, K. L. Endosomal Escape and siRNA Delivery with Cationic Shell Crosslinked Knedel-like Nanoparticles with Tunable Buffering Capacities. *Biomaterials* **2012**, *33*, 8557–8568.
20. Ferrer-Miralles, N.; Vázquez, E.; Villaverde, A. Membrane-Active Peptides for Non-Viral Gene Therapy: Making the Safest Easier. *Trends Biotechnol.* **2008**, *26*, 267–275.
21. Shim, M. S.; Kwon, Y. J. Controlled Delivery of Plasmid DNA and siRNA to Intracellular Targets using Ketalized Polyethylenimine. *Biomacromolecules* **2008**, *9*, 444–455.
22. Tallafuss, A.; Gibson, D.; Morcos, P.; Li, Y.; Seredick, S.; Eisen, J.; Washbourne, P. Turning Gene Function ON and OFF using Sense and Antisense Photo-morpholinos in Zebrafish. *Development* **2012**, *139*, 1691–1699.
23. Ando, H.; Furuta, T.; Tsien, R. Y.; Okamoto, H. Photo-mediated Gene Activation using Caged RNA/DNA in Zebra- fish Embryos. *Nat. Genet.* **2001**, *28*, 317–325.
24. Mikat, V.; Heckel, A. Light-Dependent RNA Interference with Nucleobase-Caged siRNAs. *RNA* **2007**, *13*, 2341–2347.
25. Shah, S.; Jain, P. K.; Kala, A.; Karunakaran, D.; Friedman, S. H. Light-Activated RNA Interference using Double-Stranded siRNA Precursors Modified using a Remarkable Regiospecificity of Diazo-based Photolabile Groups. *Nucleic Acids Res.* **2009**, *37*, 4508–4517.
26. Berg, K.; Selbo, P. K.; Prasmickaite, L.; Tjelle, T. E.; Sandvig, K.; Moan, J.; Gaudernack, G.; Fodstad, Ø.; Kjølsrud, S.; Anholt, H. Photochemical Internalization: a Novel Technology for Delivery of Macromolecules into Cytosol. *Cancer Res.* **1999**, *59*, 1180–1183.
27. Oliveira, S.; Fretz, M. M.; Høgset, A.; Storm, G.; Schiffelers, R. M. Photochemical Internalization Enhances SIlencing of Epidermal Growth Factor Receptor Through Improved Endosomal Escape of siRNA. *Biochim. Biophys. Acta, Biomembr.* **2007**, *1768*, 1211–1217.
28. Selbo, P. K.; Sandvig, K.; Kirveliene, V.; Berg, K. Release of Gelonin from Endosomes and Lysosomes to Cytosol by Photochemical Internalization. *Biochim.Biophys. Acta, Gen. Subj.* **2000**, *1475*, 307–313.
29. Mellert, K.; Lamla, M.; Scheffzek, K.; Wittig, R.; Kaufmann, D. Enhancing Endosomal Escape of Transduced Proteins by Photochemical Internalisation. *PloS One* **2012**, *7*, e52473.
30. Adigbli, D.; MacRobert, A. Photochemical Internalisation: The Journey from Basic Scientific Concept to the Threshold of Clinical Application. *Curr. Opin. Pharmacol.* **2012**, *12*, 434–438.
31. Bøe, S.; Prasmickaite, L.; Engesæter, B.; Hovig, E. Light-directed Delivery of Nucleic Acids. In *Therapeutic Oligonucleotides*; Springer: Berlin, 2011; pp 107−121.
32. Idris, N. M.; Li, Z.; Ye, L.; Wei Sim, E. K.; Mahendran, R.; Ho, P. C.-L.; Zhang, Y. Tracking Transplanted Cells in Live Animal using Upconversion Fluorescent Nanoparticles. *Biomaterials* **2009**, *30*, 5104–5113.
33. Yang, Y.; Liu, F.; Liu, X.; Xing, B. NIR Light Controlled Photorelease of siRNA and its Targeted Intracellular Delivery Based on Upconversion Nanoparticles. *Nanoscale* **2013**, *5*, 231–238.
34. Idris, N. M.; Gnanasammandhan, M. K.; Zhang, J.; Ho, P. C.; Mahendran, R.; Zhang, Y. *In vivo* Photodynamic Therapy using Upconversion Nanoparticles as Remote-Controlled Nanotransducers. *Nat. Med.* **2012**, *18*, 1580–1585.
35. Jayakumar, M. K. G.; Idris, N. M.; Zhang, Y. Remote Activation of Biomolecules in Deep Tissues using Near-Infrared-to-UV Upconversion Nanotransducers. *Proc. Natl. Acad. Sci. U.S.A.* **2012**, *109*, 8483–8488.
36. Wang, C.; Cheng, L.; Liu, Z. Drug Delivery with Upconversion Nanoparticles for Multi-Functional Targeted Cancer Cell Imaging and Therapy. *Biomaterials* **2011**, *32*, 1110–1120.
37. Iversen, T.-G.; Skotland, T.; Sandvig, K. Endocytosis and Intracellular Transport of Nanoparticles: Present Knowledge and Need for Future Studies. *Nano Today* **2011**, *6*, 176–185.
38. Qian, H. S.; Guo, H. C.; Ho, P. C. L.; Mahendran, R.; Zhang, Y. Mesoporous-Silica-Coated Up-conversion Fluorescent Nanoparticles for Photodynamic Therapy. *Small* **2009**, *5*, 2285–2290.
39. Park, I. Y.; Kim, I. Y.; Yoo, M. K.; Choi, Y. J.; Cho, M.-H.; Cho, C. S. Mannosylated Polyethylenimine Coupled Mesoporous Silica Nanoparticles for Receptor-Mediated Gene Delivery. *Int. J. Pharm.* **2008**, *359*, 280–287.
40. Slowing, I. I.; Vivero-Escoto, J. L.; Wu, C.-W.; Lin, V. S.-Y. Mesoporous Silica Nanoparticles as Controlled Release Drug Delivery and Gene Transfection Carriers. *Adv. Drug Delivery Rev.* **2008**, *60*, 1278–1288.
41. Berg, K.; Høgset, A.; Prasmickaite, L.; Weyergang, A.; Bonsted, A.; Dietze, A.; Lou, P.-J.; Bown, S.; Norum, O.-J.; Møllergård, H. M. T.; Selbo, P. K. Photochemical Internalization (PCI): a Novel Technology for Activation of Endocytosed Therapeutic Agents. *Med. Laser Appl.* **2006**, *21*, 239–250.
42. Alshamsan, A.; Hamdy, S.; Haddadi, A.; Samuel, J.; El-Kadi, A. O.; Uludağ, H.; Lavasanifar, A. STAT3 Knockdown in B16 Melanoma by siRNA Lipopolyplexes Induces Bystander Immune Response *in Vitro* and *in Vivo*. *Transl. Oncol.* **2011**, *4*, 178–188.
43. Emeagi, P.; Maenhout, S.; Dang, N.; Heirman, C.; Thielemans, K.; Breckpot, K. Downregulation of STAT3 in Melanoma: Reprogramming the Immune Microenvironment as an Anticancer Therapeutic Strategy. *Gene Ther.* **2013**, *20*, 1085–1092.
44. Slowing, I. I.; Vivero-Escoto, J. L.; Zhao, Y.; Kandel, K.; Peeraphatdit, C.; Trewyn, B. G.; Lin, V. S. Y. Exocytosis of Mesoporous Silica Nanoparticles from Mammalian Cells: from Asymmetric Cell-to-Cell Transfer to Protein Harvesting. *Small* **2011**, *7*, 1526–1532.
45. Goldberg, M. S.; Xing, D.; Ren, Y.; Orsulic, S.; Bhatia, S. N.; Sharp, P. A. Nanoparticle-Mediated Delivery of siRNA Targeting Parp1 Extends Survival of Mice Bearing Tumors Derived from Brca1-Deficient Ovarian Cancer Cells. *Proc. Natl. Acad. Sci. U.S.A.* **2011**, *108*, 745–750.
46. Li, S.-D.; Chen, Y.-C.; Hackett, M. J.; Huang, L. Tumor-Targeted Delivery of siRNA by Self-Assembled Nanoparticles. *Mol. Ther.* **2008**, *16*, 163–169.
47. Liu, J.; Bu, W.; Pan, L.; Shi, J. NIR-Triggered Anticancer Drug Delivery by Upconverting Nanoparticles with Integrated Azobenzene-Modified Mesoporous Silica. *Angew. Chem., Int. Ed.* **2013**, *52*, 4375–4379.
48. Liu, J.; Bu, W.; Zhang, S.; Chen, F.; Xing, H.; Pan, L.; Zhou, L.; Peng, W.; Shi, J. Controlled Synthesis of Uniform and Monodisperse Upconversion Core/Mesoporous Silica Shell Nanocomposites for Bimodal Imaging. *Chem.—Eur. J.* **2012**, *18*, 2335–2341.
49. Su, F.; Kozak, K. R.; Imaizumi, S.; Gao, F.; Amneus, M. W.; Grijalva, V.; Ng, C.; Wagner, A.; Hough, G.; Farias-Eisner, G. Apolipoprotein AI (apoA-I) and ApoA-I Mimetic Peptides Inhibit Tumor Development in a Mouse Model of Ovarian Cancer. *Proc. Natl. Acad. Sci. U.S.A.* **2010**, *107*, 19997–20002.
50. Muscella, A.; Vetrugno, C.; Migoni, D.; Biagioni, F.; Fanizzi, F.; Fornai, F.; De Pascali, S.; Marsigliante, S. Antitumor Activity of [Pt(*O,O'*-acac)(γ-acac)(DMS)] in Mouse Xeno-Graft Model of Breast Cancer. *Cell Death Dis.* **2014**, *5*, e1014.